ORIGINAL RESEARCH

American Heart Association | American Stroke Association

A Brain Phenotype for Stressor-Evoked Blood Pressure Reactivity

Peter J. Gianaros, PhD; Lei K. Sheu, PhD; Fatma Uyar, PhD; Jayanth Koushik, BS; J. Richard Jennings, PhD; Tor D. Wager, PhD; Aarti Singh, PhD; Timothy D. Verstynen, PhD

***Background*—**Individuals who exhibit large-magnitude blood pressure (BP) reactions to acute psychological stressors are at risk for hypertension and premature death by cardiovascular disease. This study tested whether a multivariate pattern of stressor-evoked brain activity could reliably predict individual differences in BP reactivity, providing novel evidence for a candidate neurophysiological source of stress-related cardiovascular risk.

***Methods and Results*—**Community-dwelling adults (N=310; 30–51 years; 153 women) underwent functional magnetic resonance imaging with concurrent BP monitoring while completing a standardized battery of stressor tasks. Across individuals, the battery evoked an increase systolic and diastolic BP relative to a nonstressor baseline period (M Δsystolic BP/Δdiastolic BP=4.3/1.9 mm Hg [95% confidence interval=3.7–5.0/1.4–2.3 mm Hg]). Using cross-validation and machine learning approaches, including dimensionality reduction and linear shrinkage models, a multivariate pattern of stressor-evoked functional magnetic resonance imaging activity was identified in a training subsample (N=206). This multivariate pattern reliably predicted both systolic BP (r=0.32; P<0.005) and diastolic BP (r=0.25; P<0.01) reactivity in an independent subsample used for testing and replication (N=104). Brain areas encompassed by the pattern that were strongly predictive included those implicated in psychological stressor processing and cardiovascular responding through autonomic pathways, including the medial prefrontal cortex, anterior cingulate cortex, and insula.

***Conclusions*—**A novel multivariate pattern of stressor-evoked brain activity may comprise a phenotype that partly accounts for individual differences in BP reactivity, a stress-related cardiovascular risk factor. **(*J Am Heart Assoc*. 2017;6:e006053. DOI: 10.1161/JAHA.117.006053.)**

Key Words: cardiovascular reactivity • functional magnetic resonance imaging • machine learning • mental stress • psychology and behavior • stress

Acute psychological stressors evoke rapid cardiovascular reactions, including rises in heart rate (HR) and blood pressure (BP). These stressor-evoked reactions provide presumptive hemodynamic and metabolic support for adaptive and defensive behavioral action (eg, fight-or-flight).[1] Individuals differ, however, in the extent to which they exhibit stressor-evoked cardiovascular reactivity. Some have a reliable tendency to exhibit large-magnitude, or "exaggerated," stressor-evoked cardiovascular reactions that disproportionately exceed the metabolic demands engendered by a given psychological stressor.[2–4] Compared with their less reactive counterparts, individuals exhibiting a phenotype for exaggerated stressor-evoked cardiovascular reactivity—especially *BP* reactivity—are at greater risk for future hypertension, an accelerated progression of preclinical atherosclerosis, and cardiovascular disease (CVD) mortality.[5–7] Moreover, the risk conferred by stressor-evoked cardiovascular reactivity is unaccounted for by conventional risk factors for CVD.[5] Accordingly, understanding the sources of stressor-evoked cardiovascular reactivity is relevant for determining the mechanisms of stress-related CVD risk.

Acute stressor-evoked cardiovascular reactions arise from proximal changes in autonomic nervous system outflow to the heart and vasculature, typified by increases in the activity of the sympathetic limb and decreases in the parasympathetic limb of the autonomic nervous system.[8] These autonomic changes are generated and regulated by evolutionarily

From the Department of Psychology (P.J.G., L.K.S.) and Departments of Psychology and Psychiatry (J.R.J.), University of Pittsburgh, Pittsburgh, PA; Center for the Neural Basis of Cognition, University of Pittsburgh and Carnegie Mellon University, Pittsburgh, PA (P.J.G., T.D.V.); Department of Psychology (F.U., T.D.V.) and Machine Learning Department (J.K., A.S.), Carnegie Mellon University, Pittsburgh, PA; Departments of Psychology and Neuroscience, University of Colorado at Boulder, CO (T.D.W.).

Accompanying Tables S1 through S4 and Figure S1 are available at http://jaha.ahajournals.org/content/6/9/e006053/DC1/embed/inline-supplementary-material-1.pdf

Correspondence to: Peter J. Gianaros, PhD, Department of Psychology, 3131 Sennott Sq, 210 S Bouquet St, Pittsburgh, PA 15260-9150. E-mail: gianaros@pitt.edu

Received March 10, 2017; accepted July 7, 2017.

Clinical Perspective

What Is New?

- People with a tendency to exhibit exaggerated (metabolically excessive) blood pressure reactions to psychological stressors are at risk for hypertension, adverse clinical cardiovascular events, and premature cardiovascular mortality.
- Exaggerated blood pressure reactions to psychological stressors may be determined, in part, by a "brain phenotype" that is characterized by reliable neural activity changes in brain areas that regulate cardiovascular physiology during stressful experiences.

What Are the Clinical Implications?

- Brain phenotypes determined by neuroimaging methodologies could be used in translational efforts to better monitor, predict, and possibly reduce stress-related risk for cardiovascular disease.

conserved brain areas.[9–11] Collectively, these areas are referred to as a "central autonomic network" or, more inclusively, as brain areas for visceral control.[12–14] Based on human functional neuroimaging research, animal models, and patient lesion studies, brain areas for visceral control encompass cell groups within the medial and orbital prefrontal cortex, anterior cingulate cortex, insula, hippocampus, extended amygdala, thalamus, hypothalamus, periaqueductal gray, pons, and medulla.[13,15–19] Distributed patterns of neural signaling among these brain areas regulate autonomic nervous system activity to coordinate hemodynamic function with behavior across a range of contexts and experiences, especially those that are appraised by individuals as psychologically stressful.[13] In this regard, brain areas for visceral control may provide a substrate for centrally orchestrating behavioral and stress-related influences on CVD risk through autonomic and hemodynamic mechanisms. An expanding corpus of research supports this possibility: Patterns of functional activity within brain areas for visceral control have been related in meta-analyses of human neuroimaging studies to stressor-evoked cardiovascular reactivity, as well as indicators of autonomic cardiovascular control and other systemic physiological markers of CVD risk.[12,13,18,19] Thus, individual differences in the functionality of brain areas for visceral control may correspond to a central nervous system source of variability in stressor-evoked cardiovascular reactivity and possible vulnerability to stress-related CVD risk.

At present, however, there are several problematic features of existing human neuroimaging studies on the putative central nervous system (brain) bases of individual differences in stressor-evoked cardiovascular reactivity (eg, BP reactivity). These features not only limit our understanding of the brain mechanisms of stressor-evoked cardiovascular reactivity, but also the broader clinical and translational use of functional neuroimaging methods in stress-related CVD research. Specifically, neuroimaging methods, particularly functional magnetic resonance imaging (fMRI), are well suited for testing whether variability in stressor-evoked cardiovascular reactivity is predicted by variability in brain activation to psychological stressors. Precisely determining this "brain-body" or "brain-physiology" relationship, however, requires moving beyond standard neuroimaging analysis approaches. First and foremost, typical fMRI analysis approaches test the degree to which a location in the brain (eg, a voxel) is active, given that a particular feature variable is present (eg, the likelihood of a voxel changing in activity given the presence of a stressor).[20] This approach, however, suffers from 2 critical problems: First, the analysis is typically implemented on a voxel-by-voxel basis, resulting in a massive multiple statistical testing problem when applied to all voxels in the brain. Second, in the context of predicting a given response (eg, BP reactivity) from brain activity, the direction of the statistical problem needs to be reversed: Hence, the analysis must determine the likelihood of a response variable, such as BP reactivity, *given* a collection of voxel activity patterns distributed across the brain. Critically, this reversal dramatically increases the dimensionality of the problem, because the number of voxels measured in the brain (ie, predictor variables) is much larger than the typical number of participants in most fMRI studies. Another limitation of conventional fMRI analytics is that they rarely test the predictive utility of a given model on an independent test sample. This undermines the ability to determine whether an observed brain-physiology association will generalize to different groups of people, which, in turn, constrains inferences about reliability, generalizability, and the magnitude of effect sizes across contexts.[21,22] Overcoming these limitations in conventional fMRI analysis with multivariate and cross-validation methods, however, allows for identifying generalizable "brain phenotypes" for stressor-evoked BP reactivity that could be broadly applied and tested in future translational research on at-risk individuals and clinical patient samples.

In the present study, we thus used a whole-brain and pattern-based machine learning approach in a sample of over 300 midlife adults who completed a standardized stressor battery during neuroimaging by fMRI with simultaneous BP monitoring. Using a cross-validation approach, we first derived a multivariate model that was trained to predict BP reactivity from stressor-evoked fMRI activity across the entire brain in a subsample of 206 participants. This approach combined principal component analysis and a least absolute shrinkage and selection operator (LASSO) regression to accommodate the high dimensionality of the prediction

problem (ie, a large number of predictors relative to the sample size). This LASSO/principal components regression approach produced a unique multivariate brain pattern, a brain phenotype map, that reflected each voxel's multivariate and weighted contribution to predicting BP reactivity. To test for generalizability, reliability, and accuracy of the trained model, the multivariate brain pattern was then used to predict BP reactivity in a separate subsample of 104 participants who were *not* used for training. Finally, we tested the performance of the multivariate pattern to explicitly predict BP reactivity and not other (eg, behavioral, self-report) dimensions of acute stress reactivity. To our awareness, this is the largest neurophysiological study of stressor-evoked BP reactivity and the first to apply cross-validation methods to characterize a putative brain phenotype for this particular stress-related predictor of CVD risk.

Methods

Participants

Participants were 331 men (N=165) and women (N=166) aged 30 to 51 years from the Pittsburgh Imaging Project (PIP), an ongoing longitudinal study of the neurophysiological correlates of CVD risk. Here we report results from planned (a priori) tests of baseline associations between fMRI activity and stressor-evoked BP reactivity. Future planned reports will focus on fMRI activity and the longitudinal progression of preclinical CVD risk factors. Exclusionary criteria included: (1) any history of clinical CVD or a CVD event (including stage II hypertension, stroke, myocardial infarction, congestive heart failure, or arrhythmia); (2) cardiovascular surgery; (3) cancer, a chronic kidney or liver condition, type 1 or 2 diabetes mellitus, or any pulmonary or respiratory disease; (4) current or past psychiatric diagnoses of substance abuse or mood disorders; (5) cerebrovascular trauma; (6) neurosurgery or any neurological condition; (7) pregnancy (verified by urine test in females); (8) color-blindness; (9) claustrophobia; (10) ferromagnetic implants; or (11) any use of psychotropic, lipid-lowering, weight loss, insulin, glucocorticoid, hypoglycemic, or cardiovascular medications. All participants provided their informed consent to complete study protocols, which were approved by the University of Pittsburgh (Pittsburgh, PA) Institutional Review Board.

Recruitment and Missing Data

Mass mailings were used to recruit community-dwelling adults residing in southwestern Pennsylvania from August 2008 to October 2014, and data collection for measures in the current report spanned this time period. Initial phone screening of those responding to the mailings yielded 754 potentially eligible respondents, of whom 460 appeared for in-person screening. Of these, 129 were ineligible, declined to participate before consenting, or withdrew because of de novo ineligibility or personal reasons (eg, pregnancy, residential relocation, etc). This resulted in a final sample of 331 individuals who completed all baseline assessment protocols. After quality-control review, 157 men and 153 women were determined to have complete and useable data, for an effective analytic sample of N=310 in the current report. Reasons for exclusion included unusable fMRI imaging data (eg, because of excessive movement artifacts), failure to comply with study protocols, and data acquisition failure during cardiovascular monitoring. There were no statistically significant differences in the demographic composition (ie, age, sex, race, and self-reported ethnicity) of those comprising the analytical sample (N=310) and those with missing data (N=21). Table provides summary characteristics of the analytical study sample.

MRI Protocol

Participants refrained from eating, exercising, and consuming caffeinated and tobacco products, as well as drinking alcoholic beverages, for at least 8 hours before MRI testing in the morning (7:00 to 11:00 AM). At testing, they underwent a medical history and screening interview, followed by a blood draw to assess fasting serum markers of CVD risk (ie, glucose, total cholesterol, high-density lipoprotein levels, and triglyceride concentrations), as well as anthropometric measures (eg, height, weight, and waist circumference), demographic and psychosocial information, and seated BP (see Table for descriptive statistics). Thereafter, participants were provided with instructions about the MRI tasks described below, and they practiced these tasks before MRI. For MRI, participants were first fitted with a BP cuff matched to arm size, inserted into the MRI scanner, and asked to rest for ≈20 minutes. Participants then completed 2 stressor tasks with concurrent functional MRI (fMRI) and BP monitoring (see below).

MRI Data Acquisition

MRI data were acquired on a 3 Tesla Trio TIM whole-body scanner (Siemens, Erlangen, Germany), equipped with a 12-channel head coil. Functional blood-oxygen-level–dependent (BOLD) images were acquired with a gradient echo-planar imaging sequence by these parameters: time to repetition/time to echo=2000/28 ms; matrix resolution=64×64; field of view=205×250 mm; slice thickness=3 mm (no gap); and flip angle=90°. For anatomical coregistration of fMRI images and assessments of brain morphology, T_1-weighted 3-dimensional magnetization-prepared rapid gradient echo neuroanatomical images were acquired by these parameters: time to repetition/

Table. Sample Characteristics and Descriptive Statistics (N=310; 157 Men, 153 Women)

	Mean or (%)	SD or 95% CI
Characteristic		
Age, y	40.3	6.3
Race, %		
White	70.7	
Black	23.2	
Multiple	6.1	
Body mass index, kg/m^2	26.8	5.0
Total cholesterol, mg/dL	183.9	32.4
Triglycerides, mg/dL	94.5	58.1
HDL, mg/dL	50.8	16.3
Glucose, mg/dL	88.7	10.9
Number of school years completed	16.7	3.3
Seated resting SBP, mm Hg	120.6	9.8
Seated resting DBP, mm Hg	72.4	8.5
Smoking status, %		
Current	16.8	
Former	19.7	
Never	63.6	
Depressive symptoms (BDI-II)	3.5	3.5
Trait anxiety (STAI-T)	32.9	7.4
Trait hostility (CMHS-T)	14.1	7.6
Task accuracy (% correct)		
MSIT congruent condition	91.4	6.9
MSIT incongruent condition	56.7	7.9
Stroop congruent condition	84.5	9.6
Stroop incongruent condition	55.5	10.3
Task reaction time, ms		
MSIT congruent condition	542.7	116.7
MSIT incongruent condition	900.1	202.4
Stroop congruent condition	1300.3	297.1
Stroop incongruent condition	1870.0	470.7
Change from baseline in valence		
MSIT	−1.1	(−1.3, −0.9)
Stroop	−1.6	(−1.8, −1.3)
Change from baseline in arousal		
MSIT	2.6	(2.3, 2.8)
Stroop	3.1	(2.8, 3.3)
Change from baseline in SBP, mm Hg		
MSIT	3.5	(2.9, 4.1)
Stroop	5.0	(4.2, 5.7)
Change from baseline in DBP, mm Hg		
MSIT	1.4	(0.9, 1.9)
Stroop	2.2	(1.6, 2.8)
Change from baseline in HR, bpm		
MSIT	6.2	(5.6, 6.7)
Stroop	8.1	(7.4, 8.8)

Data are presented as number (percentage), mean±SD, or mean and 95% confidence interval (CI). BDI-II indicates Beck Depression Inventory-II; CMHS-T, Cook-Medley Hostility Inventory-Trait version; DBP, diastolic blood pressure; HDL, high-density lipoproteins; LDL, low-density lipoproteins; MSIT, Multi-Source Interference Task; SBP, systolic blood pressure; STAI-T, State-Trait Anxiety Inventory-Trait version.

time to echo=2100/3.29 ms; time to inversion=1100 ms; matrix resolution=256×208; field of view=256×208 mm; slice thickness=1 mm (no gap); flip angle=8°. Resting cerebral blood flow (CBF) images were acquired with a pulsed arterial spin-labeling sequence using a flow-sensitive alternating inversion recovery method,[23] specifically applying a saturation pulse 700 ms after an inversion pulse. To reduce transit artifacts, a 1000-ms delay separated the end of the labeling pulse and the time of image acquisition. Resting cerebral blood flow (CBF) image acquisition parameters were: field of view=240×240 mm; matrix size=64×64; time to repetition=4 seconds; time to echo=18 ms; and flip angle=90°. Twenty-one slices (5 mm thick, 1 mm gap) were acquired sequentially in an inferior-to-superior direction, yielding 80 total CBF images (40 labeled, 40 unlabeled; 2 initial discarded images allowing for magnetic equilibration).

fMRI Stressor Battery

The stressor battery is publically available at http://bnl.pitt.edu/resources.html and has been detailed.[24] The battery includes a Stroop task and a modified Multi-Source Interference Task (MSIT). Both entail conflict, negative feedback, and responding under time pressure to unpredictable and uncontrollable stimuli, modeling canonical elements of a stressful experience.[13] Briefly, participants completed 4, 52- to 60-second blocks of trials in both tasks defining a congruent condition, which were interleaved with 4, 52- to 60-second blocks of trials defining an incongruent condition. Conditions were preceded by a 10- to 17-second fixation period. In the Stroop, participants selected colors of target words by choosing 1 of 4 identifier words using buttons on a glove that matched identifier words on the screen (eg, thumb button 1=word on left, etc). For congruent trials: (1) targets were in colors congruent with target words, and (2) identifiers were in the same colors as targets. For incongruent trials: (1) targets

were in colors incongruent with targets, and (2) identifiers were in colors incongruent with colors that the identifiers name. In the MSIT, participants selected a number that differed from 2 others by pressing 1 of 3 buttons on the glove that matched a number on the screen (thumb button 1=number 1, etc). For congruent trials, target positions were compatible with their glove positions. For incongruent trials, target positions were incompatible with their glove positions. In incongruent conditions of *both* tasks, accuracy was titrated by altering intertrial intervals to control for individual differences in task engagement. Thus, consecutive accurate choices shortened intertrial intervals. To control for motor response differences between conditions, the number of trials in the congruent condition was yoked to total completed in the incongruent condition. For yoking, (1) an incongruent block was run first and (2) congruent condition trials appeared at the mean intertrial interval of the previous incongruent block. During the practice protocol before MRI, there was no performance titration or yoking implemented for either task to reduce the likelihood of habituation. We have previously established that this battery evokes reliable individual differences in cardiovascular, self-report, and functional neural responding over a period of ≈88 days, with test-retest reliability coefficients of 0.57 to 0.87 across domains of stressor responding.[24]

Stressor Battery Performance and Subjective Ratings

Task performance (accuracy) during the battery was computed as the percentage of trials correctly completed. Post hoc, we confirmed the successful titration of accuracy: Mean accuracy during the incongruent condition of the tasks was titrated across participants to 56.1% (±9.1% SD), and mean accuracy increased by 31.9% (95% confidence interval [CI] =30.7–33.1) during the congruent condition (see Table for descriptive statistics for each task). In this way, individual differences in task performance were experimentally controlled. In conjunction with titration-induced accuracy changes, mean response times to trials delivered during the incongruent condition compared with the congruent condition of each task were slowed by an average of 106 ms (95% CI=86.6–125.6). To assess ratings of valence (1=very pleasant; 9=very unpleasant) and arousal (1=very calm; 9=very aroused), participants completed a modified Self-Assessment Manikin scale[25] after the resting (prestressor) period and each task. As a manipulation check, we verified that participants reported feeling less pleasant and more aroused during the tasks (paired *t* test t-values ranged from 10.3 to 19.4; *Ps*≤0.001). For ancillary analyses, participants also completed psychosocial inventories to assess suspected correlates of CVD risk, namely: depressive symptoms by the Beck Depression Inventory-II[26]; dispositional anxiety by the State-Trait Anxiety Index[27]; and hostility by the Cook-Medley Hostility Inventory.[28,29]

Cardiovascular Monitoring and BP

Participants' average seated resting BP was systolic BP/diastolic BP (SBP/DBP)=120.6/72.4 mm Hg (±9.8/8.5 mm Hg SD), as determined by the mean of the last 2 BP readings obtained on 2 separate testing visits with an oscillometric device (Critikon Dinamap 8100; Johnson & Johnson, Tampa, FL) and taken 2 minutes apart after a 20-minute acclimation period (BP cuffs matched to arm size).

During MRI, participants' BP and HR were measured during the resting (prestressor) and stressor battery periods from the brachial artery of the arm that was not used for task responding. All participants used their right hand to complete the tasks and provide ratings. There were 3 participants who were identified as left-handed, as verified by the Edinburgh Handedness Questionnaire.[30] Before testing, these participants reported that they were able to use the right-hand response glove for the task protocol. For protocol consistency across participants, they were allowed to do so, and we recorded BP from their left arm. By independent-samples *t* tests, their task performance (accuracy, reaction time) and cardiovascular (SBP, DBP, and HR) reactivity did not differ significantly from the rest of the sample (all *Ps*>0.423). BP measurements were obtained with an oscillometric device (Multigas 9500; MedRad Inc., Warrendale, PA), set to inflate every 2.5 minutes during the prestressor period and once during each condition of the Stroop task and MSIT. To compute prestressor BP and HR, the final 3 measurements from the prestressor period were averaged. The incongruent condition—minus—resting BP/HR change scores (ΔBP, ΔHR) were used to compute cardiovascular reactivity to match our previous work.[31,32] These change (reactivity) scores averaged over the Stroop and MSIT tasks were used in analyses given the high correlations between task reactivity scores (Figure 1).

MRI Data Processing

BOLD fMRI data from the Stroop and MSIT tasks were processed using Statistical Parametric Mapping (SPM) software, version 8 (SPM8; http://www.fil.ion.ucl.ac.uk/spm/). For each task, the time series of 280 volumes of BOLD images were realigned to the first image, corrected for motion distortion, and normalized to Montreal Neurological Institute space. Normalized images were rescaled (2-mm isotropic voxels) and smoothed with a 6-mm full width at half maximum Gaussian kernel. At the individual level, incongruent versus congruent condition task effects on fMRI signal

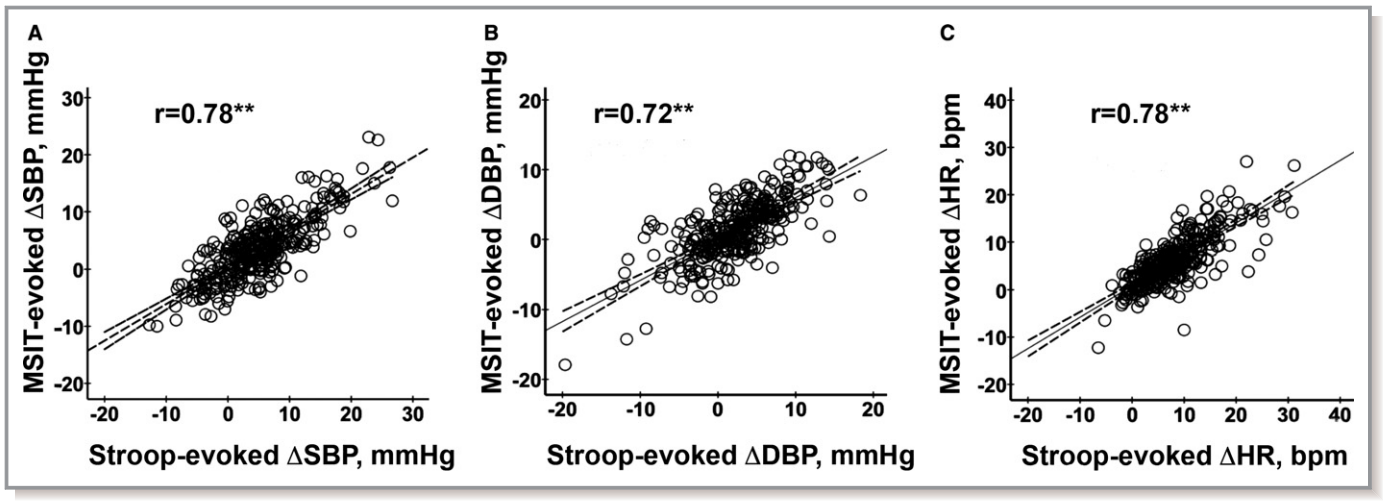

Figure 1. The Stroop task and Multi-Source Interference Task (MSIT) evoked comparable patterns of cardiovascular reactivity across individuals. A, Comparison of systolic blood pressure (SBP), (B) diastolic blood pressure (DBP), and (C) heart rate (HR) reactivity values across tasks.

changes were estimated by general linear modeling, in which the conditions were modeled by boxcar functions convolved with the default hemodynamic response function. Motion parameters generated from realignment were also included as covariates at the individual level to account for nuisance variance in the BOLD signal attributable to head movement. Before general linear modelings, a high-pass filter of 187 seconds was applied to the fMRI BOLD signal time series to filter low-frequency artifacts. All images were screened using the Artifact Detection Toolbox (ART; http://web.mit.edu/swg/software.htm), including screening for movement artifact and signal loss. Covariation between task conditions and movement parameters was also tested to ensure that condition effects were not confounded with movement: We observed no statistically significant correlations (all *P*s>0.30). Finally, to minimize the contribution of any extreme values in the fMRI BOLD signal time series, we implemented the weighted least-squares algorithm using the RobustWLS toolbox in SPM8.[33]

Stressor-evoked brain activation was estimated by the statistical contrast of BOLD signal activity during the incongruent versus congruent condition in each task of the stressor battery. Resulting contrast maps were then averaged over the 2 tasks to conform with previous work, match the cardiovascular reactivity computation approach described above, minimize measurement error, and increase reliability.[24] Accordingly, we verified the spatial similarity of the Stroop and MSIT contrast maps by the Dice coefficient, as well as the correlation of BOLD signal values from the 2 contrast maps. Before statistical analysis, individual-level and task-averaged contrast maps were masked by the SPM 25% gray matter probability map.

Multivariate Analysis of fMRI Data

We used machine learning to test the predictive association between stressor-evoked brain activity changes and stressor-evoked BP reactivity. In this approach, stressor-evoked brain activity in all gray matter voxels from the task-averaged contrast maps served as a multivariate predictor, with stressor-evoked SBP reactivity (ΔSBP) as the primary dependent variable. SBP reactivity was selected because of evidence that it is the parameter of cardiovascular stress reactivity most strongly related to CVD risk.[7,34] Conventionally, the predictive model would be as follows: $Y_{n\times 1}=X_{n\times v}\beta_{v\times 1}+\varepsilon_{n\times 1}$, where $\varepsilon_{n\times 1}$ is a random error of N (0, $\sigma^2 I_{n\times 1}$), $Y_{n\times 1}$ is the dependent variable (ΔSBP), and $X_{n\times v}$ is the matrix of concatenated incongruent versus congruent contrast maps of n participants with v voxels. In this model, $\beta_{v\times 1}$ corresponds to a whole-brain weight map of the effect of brain activity change in each voxel on the dependent variable (ΔSBP). This weight map would then be used to predict observations of the dependent variable in a new sample, $\hat{Y}_{new} = X_{new}\hat{\beta}$. However, because the sample size, n, is appreciably smaller than the number of predictors (voxels across the brain), v, the model engenders overfitting and limited accuracy in prediction because of high dimensionality.[35] In addition, predictors (eg, neighboring voxel-by-voxel stressor-evoked brain activity changes) may be correlated, resulting in multicollinearity. Given these limitations, we used a LASSO/principal components regression approach specifically designed for high-dimensional prediction problems along with cross-validation[36] to develop and train an initial multivariate model (multivariate brain pattern) and then test the performance of the pattern in a separate hold-out group (test sample) of participants (see Figure S1).

By this approach, two thirds of the participants (N=206) were randomly selected with stratification over the ΔSBP distribution for initial training and cross-validation of the multivariate brain pattern. Data from remaining participants (N=104) who were *not* used for training were subsequently used for testing prediction performance (ie, the test sample). The training and test samples did not differ significantly in any of the demographic, anthropometric, biological, psychosocial, or task-related variables reported in Table (all *P*s>0.14 by independent-sample *t* tests and chi-square analyses). The training and test samples also did not differ significantly in stressor-evoked SBP, DBP, or HR reactivity (all *P*s>0.31 by independent-sample *t* tests). Table S1 provides comparisons of the 2 samples.

In application of LASSO/principal components regression, the multivariate predictor matrix X was created in the training subsample, and it was then decomposed into 3 matrices, $X = U \sum V'$ by singular value decomposition. Matrix V contains the orthonormal eigenvectors of the covariance matrix, X′X, that form the orthogonal basis. The principal components here correspond to the projection of X on the eigenvector space, namely, P=XV, which preserves the variance of X and reduces dimensionality. We then regressed Y on P using LASSO with a regularization (shrinkage) parameter, λ. Specifically, we applied the least-angle regression algorithm[37,38] to find the value of b that minimizes the cost function, $f = ||Y - Pb||_2^2 + \lambda||b||_1$. The regularization parameter, λ, controls the selection of variables (ie, principal components) in the regression model, wherein a larger λ forces more coefficients in the regression model to be 0 and reduces (shrinks) the number of predictor variables.

During training, we applied 10-fold cross-validation to select the best λ and hence the principal components, P*, that yielded the smallest root mean square error. The root mean square error for each λ was calculated from the residual sum of squares of the 10 validation data sets (each with Ns=20 or 21) in the 10 training models (each with Ns=185 or 186). Once the variables (principal components), P*, were selected, the coefficients of the selected principal components, $\hat{b}^*_{n\times 1}$, were estimated by a linear least square regression of stressor-evoked SBP reactivity (ΔSBP) on the selected principal components using the training sample (N=206).

The best fitting model in principal components space, $\hat{b}^*_{n\times 1}$, was then projected back into voxel space using the unitary matrix, V, such that $\hat{\beta}_{v\times 1} = V_{v\times n}\hat{\beta}^*_{n\times 1}$. Here, $\hat{\beta}$ represents a weight map of the entire brain (multivariate brain pattern) reflecting how activity changes in individual voxels simultaneously contribute to the prediction of SBP reactivity. Thus, in order to predict stressor-evoked SBP reactivity in the hold-out test sample, we multiplied $\hat{\beta}$ by X_{test}, which is an mxv matrix of stressor-evoked fMRI activity changes, where m=104. The resulting $\hat{Y}_{test}$ vector provides a blind prediction of SBP reactivity for all m participants in the hold-out test sample. The predictive utility of the multivariate brain pattern ($\hat{\beta}$) was then determined as the correlation between observed and predicted SBP reactivity in the hold-out test sample.

In addition to predicting individual differences in stressor-evoked SBP reactivity, we computed receiver operation curve metrics to test the performance of the multivariate brain pattern ($\hat{\beta}$) in detecting "cut-off" or threshold SBP reactivity values. This enabled us to evaluate the sensitivity and specificity of predicting different levels of SBP reactivity across individuals. In a set of additional tests, we examined whether the whole-brain, multivariate pattern, $\hat{\beta}$, would predict individual differences in self-reported affective or arousal changes, as well as behavioral task performance. Finally, we tested whether $\hat{\beta}$ would outperform another widely used multivariate brain pattern developed for the prediction of an aversive behavioral state plausibly related to the experience of stress; namely, pain.[39] If our multivariate brain pattern, but not 1 for pain, predicts SBP reactivity, then this would provide a line of discriminative evidence that our multivariate brain pattern uniquely accounts for individual differences in a dimension of cardiovascular stress reactivity.

Ancillary Analyses

In a series of ancillary analyses, we examined the extent to which stressor-evoked BP reactivity was associated with individual differences in psychosocial and demographic factors, as well as possible fMRI confounders or interindividual variation in putative brain correlates of CVD risk: CBF and brain morphology. Total CBF (mL/100 g per minute) was computed according to previously detailed methods by our group[40] from arterial spin-labeling MRI data. Total volumes of gray matter, white matter, and cerebral spinal fluid compartments were computed from structural T_1-weighted MRI data using the FreeSurfer 5.3.0 software package (http://surfer.nmr.mgh.harvard.edu).

Statistical Significance

A statistical significance threshold of *P*<0.05 was adopted and 95% CIs were applied, where applicable.

Results

Stressor-Evoked Cardiovascular Reactivity

The incongruent condition of the 2 tasks of the stressor battery evoked an expected increase in average SBP and DBP compared with the prestressor baseline period (M Stroop ΔSBP/ΔDBP=4.95/2.21 mm Hg [95% CI=4.23–5.69/1.63–

2.77] and M MSIT ΔSBP/ΔDBP=3.47/1.39 mm Hg [95% CI=2.89–4.08/0.91–1.85]). The incongruent condition of the 2 tasks also increased average HR (M Stroop ΔHR=8.11 bpm [95% CI=7.43–8.82] and M MSIT ΔHR=6.16 bpm [95% CI=5.59–6.74]). As shown in Figure 1, there were individual differences in reactivity (changes from baseline) for both BP and HR; however, these individual differences in reactivity were strongly correlated across the 2 tasks (*r*s=0.78, 0.72, and 0.78 for ΔSBP, ΔDBP, and ΔHR, respectively; all *P*s<0.001). We thus averaged reactivity estimates across tasks for subsequent analyses to minimize error and better estimate stable (phenotypic) individual differences in stressor-evoked cardiovascular reactivity.[41]

Stressor-Evoked Functional Neural Activity

The Stroop task and MSIT engaged spatially overlapping (comparable) brain areas, as revealed by the incongruent versus congruent condition contrasts of BOLD signal activity (Dice coefficient for spatial similarity=0.80; see Figure 2). We note that the directions of BOLD signal changes (positive and negative) revealed by the incongruent versus congruent condition contrasts agree with those observed in other cognitively demanding fMRI stressors cf.,[42] including BOLD signal changes in areas that have been implicated in stressor processing and cardiovascular control by autonomic pathways (ie, medial and orbital prefrontal cortex, anterior cingulate cortex, insula, hippocampus, amygdala, thalamus, periaqueductal gray, and pons; see Table S2).[13] In parallel to findings for cardiovascular reactivity estimates above, voxel-wise fMRI BOLD signal changes for the incongruent versus congruent condition contrasts were strongly correlated across individuals (voxel-by-voxel *r* across tasks=0.88; *P*<0.0001). Accordingly, and consistent with previous work, task-averaged incongruent versus congruent condition contrast maps were used in subsequent analyses (see Figure 2C).

A Multivariate Brain Pattern (Phenotype) for SBP Reactivity

In a training sample (N=206), a 10-fold, cross-validation procedure yielded a multivariate (voxel-wise) brain pattern ($\hat{\beta}$) of stressor-evoked brain activity (incongruent versus congruent activity change) that predicted individual differences in SBP reactivity (ΔSBP; λ=0.33; root mean square error=5.58; 70 principal components retained after training). Figure 3A shows the whole-brain, predictive pattern learned on the training sample. In cross-validation, the ability of this multivariate brain pattern to predict stressor-evoked SBP reactivity was then determined by using the pattern to predict ΔSBP in the test sample (N=104). In this independent test sample, the brain pattern accounted for ≈9% of the variance in stressor-evoked SBP reactivity across individuals (*r*=0.32; *P*<0.005; Figure 3B). For illustration purposes, Figure 4 provides surface projections of brain areas along the medial wall and insula within the whole-brain multivariate pattern (which was used for prediction) that exhibited relatively stronger associations with ΔSBP across individuals, as determined by nonparametric permutation testing (see Tables S3 and S4 for detailed listing of areas). Again, we note that the whole-brain pattern was used for prediction and cross-validation testing.

To demonstrate that the prediction results were not sensitive to the particular individuals comprising the training and test samples, we repeated the LASSO/principal components regression analyses such that every individual was included in the test sample at least once (5-folds; training

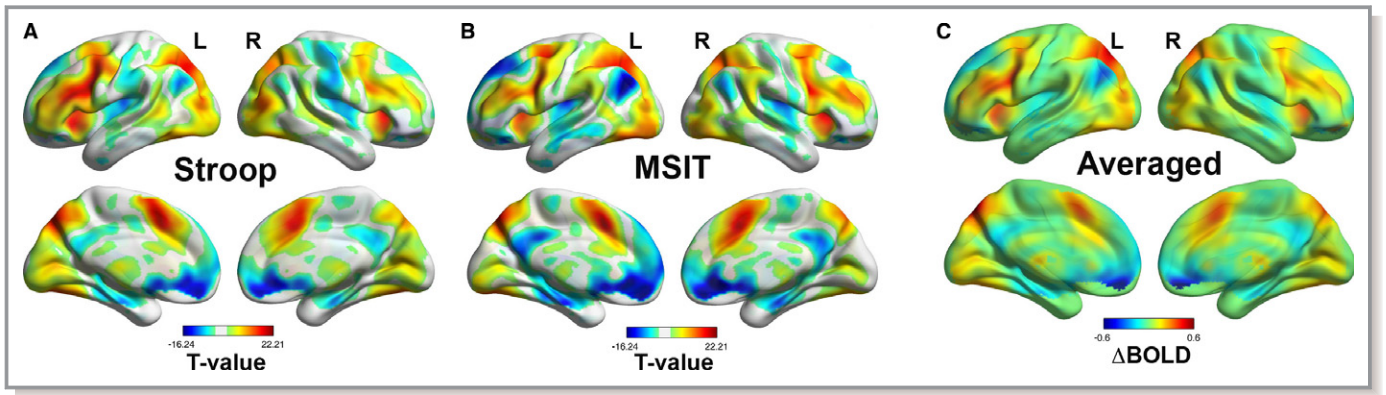

Figure 2. The Stroop task and Multi-Source Interference Task (MSIT) evoked comparable changes in brain activity (voxel-wise r of blood oxygen level dependent (BOLD) signal change=0.88; *P*<0.001; Dice coefficient for spatial overlap=0.80). Color-scaled t-statistic maps of brain areas exhibiting significant BOLD signal changes (incongruent vs congruent condition changes) are shown for the Stroop task (A) and MSIT (B). Maps in (A) and (B) correspond to statistical parametric t-statistic maps, shown at a false discovery rate threshold of 0.05 to control for multiple statistical testing. The color-scaled BOLD signal change map in (C) corresponds to the average of the Stroop and MSIT BOLD signal change maps. Task-averaged BOLD signal change maps across participants were used to generate a final and whole-brain multivariate brain pattern to predict task-averaged stressor-evoked cardiovascular reactivity.

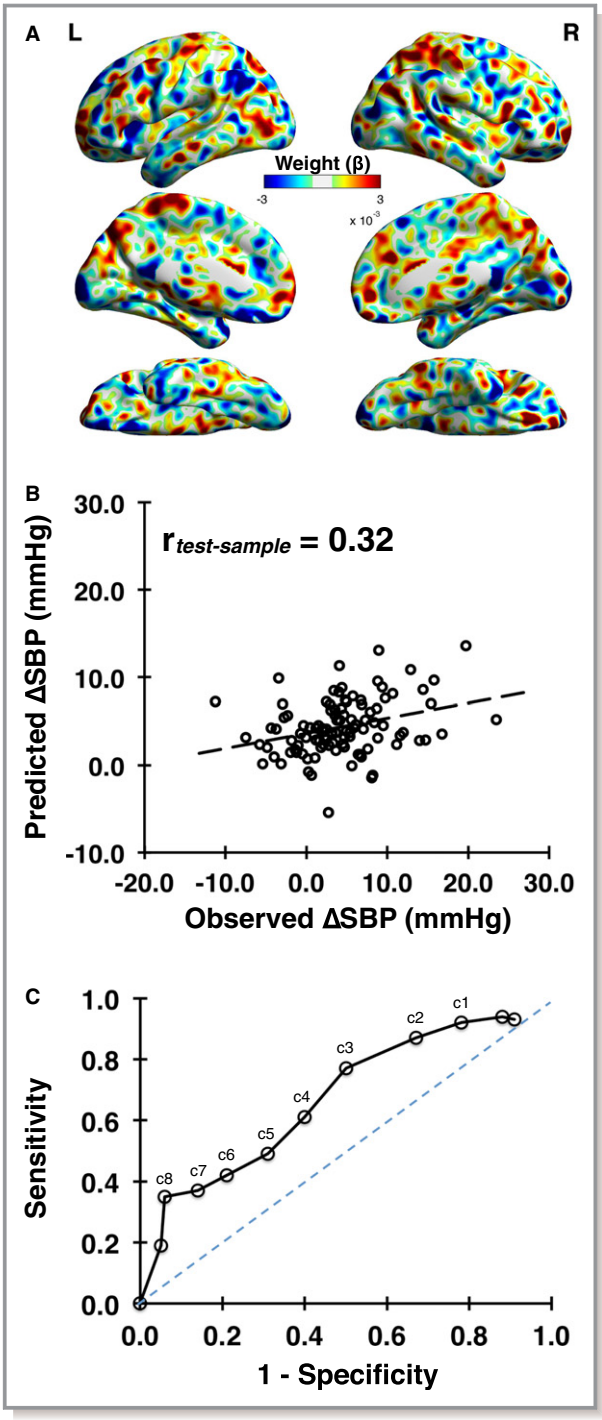

Figure 3. The final whole-brain and multivariate predictive model (weight map, $\hat{\beta}$) is shown in (A). A comparison of predicted vs observed stressor-evoked systolic blood pressure (SBP) reactivity (ΔSBP) in cross-validation using the independent test sample of N=104 (not used in training) is shown in (B), r=0.32, P=0.001. C, A receiver operating characteristic curve illustrating the sensitivity and specificity of the whole-brain multivariate pattern in predicting different cut-off values (labeled as c) of stressor-evoked SBP reactivity (ΔSBP in mm Hg) across individuals in the test sample of N=104. For example, c4 corresponds to ΔSBP of 4 mm Hg.

data set N=248 per fold; test data set N=62 per fold). The 95% CIs of the predicted versus observed correlation values in the test sample did not include zero across all 5-folds (rs=0.31±0.16, 0.35±0.18, 0.35±0.24, 0.36±0.24, and 0.30±0.23). These effect sizes were comparable to that illustrated in Figure 3B. Thus, the final cross-validation (replication) results we observed in the hold-out test sample do not appear to be sensitive to the particular individuals included in the training and test samples. Moreover, there appears to be stability in the magnitude (effect size) of the predictive association between the multivariate brain pattern and ΔSBP regardless of sample composition. Adding sex (male, female), age, and baseline (prestressor) levels of BP as covariates did not alter the direction, statistical significance, or effect sizes observed. In addition, we observed no statistically significant differences between men and women in stressor-evoked reactivity in the entire analytic sample (N=310; P>0.25). Finally, we tested whether the learned multivariate pattern might differentially predict stressor-evoked SBP reactivity among men and women. In a sex-stratified analysis in the hold-out test sample (N=104; 57 men, 47 women), the magnitude of the association between predicted and observed stressor-evoked SBP reactivity (illustrated for the entire test sample in Figure 3B) did not differ significantly between men and women (r_{men}=0.39 versus r_{women}=0.24; z=0.83; P=0.41). Accordingly, sex, age, and baseline BP were omitted from further analyses.

The receiver operation curve curve in Figure 3C illustrates sensitivity and specificity values for our multivariate brain pattern to predict different "cut offs" or "thresholds" of stressor-evoked ΔSBP (labeled with a "c" in the figure). At the approximate midpoint of this curve, for example, the true-positive rate (sensitivity) for detecting ΔSBP ≥4 mm Hg is ≈0.6, the false-positive rate (1−specificity) is ≈0.4, and the overall accuracy is ≈0.6. This midpoint value approximates the mean ΔSBP evoked by the tasks and reported above. At increasingly larger ΔSBP thresholds, detection sensitivity decreases, whereas specificity increases (eg, for predicting ΔSBP ≥5 mm Hg, sensitivity is ≈0.5, specificity is ≈0.7, and overall accuracy is ≈0.6). At increasingly greater levels of ΔSBP, however, the predictive accuracy of the multivariate pattern declines. Conversely, at smaller ΔSBP thresholds, sensitivity increases, whereas specificity decreases.

Discriminant Performance of the Multivariate Brain Pattern (Phenotype) for SBP Reactivity

We tested whether the learned multivariate brain pattern for predicting ΔSBP would also predict individual differences in stressor-evoked changes in self-reports, behavioral task performance, or other parameters of cardiovascular

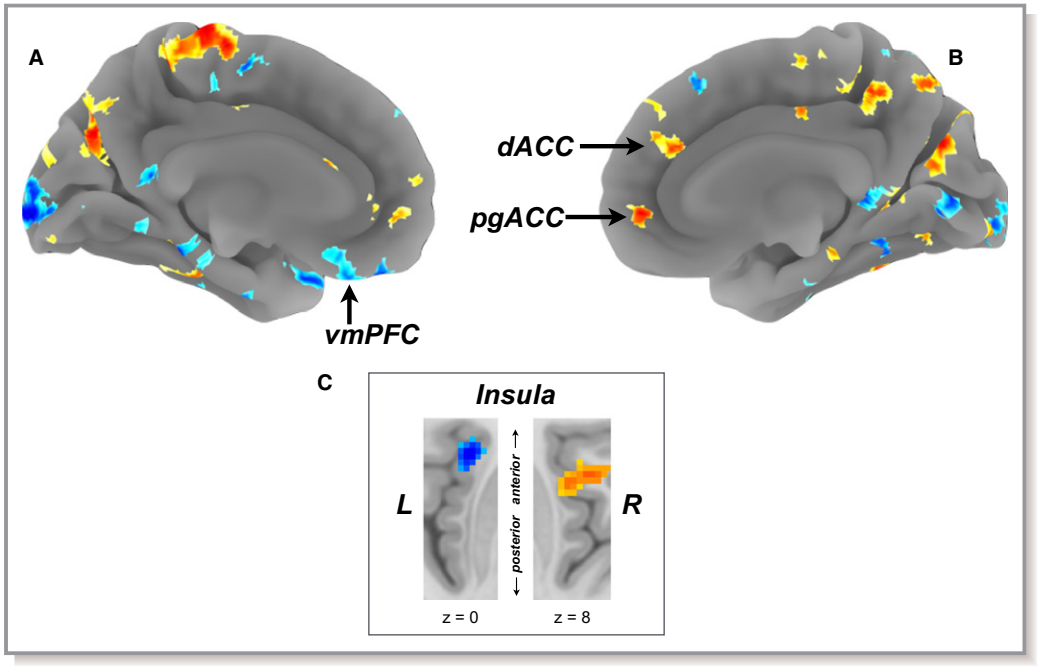

Figure 4. Multivariate pattern (weight map) used to predict stressor-evoked systolic blood pressure (SBP) reactivity. Here, the map is shown at a threshold of $P<0.05$, based on 1000 nonparametric permutations, along with an extent threshold of k=50 voxels for illustration and interpretation only (the entire whole-brain multivariate pattern was used in training and testing; see Figure 3). Warmer colors (orange/yellow) in the medial surface projections in (A) and (B) and regions of the insula shown in (C) reflect a positive predictive association between brain activity and SBP reactivity, whereas cooler colors (blue) reflect a negative association. Labeled in the medial surface projections in (A) and (B) are the ventromedial prefrontal cortex (vmPFC), perigenual anterior cingulate cortex (pgACC), and dorsal anterior cingulate cortex (dACC). Axial views of the left insula and right insula (extending into the operculum) in (C) are shown at Montreal Neurological Institute z coordinates of 0 and 8, respectively. A full listing of areas revealed after random permutation thresholding of the whole-brain multivariate pattern is in Tables S3 and S4.

physiology (ΔDBP, ΔHR) obtained during the fMRI stressor battery. We found that the brain pattern for ΔSBP did *not* reliably predict individual differences in stressor-evoked changes in effect (ratings of feeling pleasant versus unpleasant) or arousal measured by the Self-Assessment Manikin scale (r=0.04, P>0.66 for effect and r=−0.10, P>0.31 for arousal); nor did it reliably predict mean reaction time differences between the congruent and incongruent condition of the 2 stressor tasks (r=−0.01; P>0.95). The brain pattern for ΔSBP did, however, predict individual differences in stressor-evoked DBP and HR reactivity (rs=0.25 and 0.28, respectively; Ps<0.01). The latter results are likely attributed to the correlation between stressor-evoked SBP reactivity with these variables (rs=0.39–0.53; Ps<0.001), given that the multivariate brain pattern was not specifically trained to predict these other dimensions of cardiovascular reactivity. Finally, we note that the brain pattern for ΔSBP did not significantly predict *resting* SBP across individuals (r=0.09; P>0.36), suggesting specificity for *stress-related* SBP changes and not tonic (basal) levels of arterial pressure. In view of these results, the multivariate brain pattern appears to predict correlated parameters of stressor-evoked cardiovascular physiology (BP, HR), but not self-reported or behavioral measures of stressor responding.

In a final test of discriminative performance, a multivariate brain pattern developed for the prediction of self-reported pain, the neurological pain signature,[39] did not significantly predict ΔSBP across individuals (r=0.08; P>0.38). This indicates that the multivariate brain pattern derived from our training sample and evaluated in our test sample is comparatively unique in its prediction of individual differences in stressor-evoked SBP reactivity.

Ancillary Analyses

In a final series of ancillary analyses, we tested whether stressor-evoked SBP reactivity was associated with individual differences in depressive symptoms, hostility, anxiety, years of schooling, and body mass index, as well as possible confounders or putative brain or cerebrovascular correlates of CVD risk: total CBF and volumes of gray matter, white matter, and cerebral spinal fluid. We found that stressor-evoked SBP

reactivity did not significantly correlate with any of these factors (all *P*s>0.30). This suggests that the individual differences in stressor-evoked SBP reactivity that were predicted by our multivariate brain pattern are unlikely to be attributable to, or confounded by, these psychosocial, demographic, anthropometric, and cerebrovascular or brain morphology factors in this otherwise healthy and unmedicated sample.

Discussion

The main novel finding of the present study is that a whole-brain and multivariate pattern of stressor-evoked activity was reliably associated with individual differences in stressor-evoked SBP reactivity, a predictor of future hypertension, premature CVD, and CVD mortality.[5,6] This multivariate pattern, henceforth referred to as a brain phenotype for ΔSBP, was derived from the largest neuroimaging study of individual differences in cardiovascular stress reactivity to date, which integrated the use of a standardized stressor battery, cross-validation testing, and machine learning methods.[35,36,43] The brain phenotype for ΔSBP accounted for around 9% of the variance in individual differences in stressor-evoked SBP reactivity (our primary dependent variable), with overall accuracies in predicting normative SBP changes ranging from 0.6 to 0.8 (Figure 3C). Moreover, the brain phenotype exhibited discriminant performance in predicting stressor-evoked cardiovascular reactivity, insofar as it predicted correlated changes in DBP and HR reactivity, but not self-reported emotionality, arousal, or task performance changes evoked by the stressor paradigm. Finally, a different multivariate brain pattern that has been developed to predict pain,[39] an aversive behavioral state that is plausibly related to the experience of stress, did not predict individual differences in cardiovascular reactivity. The latter finding suggests some specificity for the brain pattern identified here, wherein the neural networks involved in predicting stressor-evoked cardiovascular reactivity are likely independent of those involved in both physical and subjective experiences of stress or pain. Importantly, the brain areas that were especially predictive of individual differences in stressor-evoked cardiovascular reactivity included those that are implicated in appraising psychological stressors and regulating the cardiovascular system through autonomic pathways.[12,13,44] Among other areas, these included forebrain cortical areas within the medial prefrontal cortex, anterior cingulate cortex, and insula (Figure 4; Tables S3 and S4), as well as areas of the basal ganglia, extended amygdala, hippocampus, midbrain, and cerebellum. Again, however, we emphasize that a whole-brain pattern with positive and negative weights across voxels was used for prediction and cross-validation, as opposed to individual areas. In aggregate, the present findings thus extend previous work by providing the first evidence for a candidate multivariate brain phenotype that encompasses areas across the entire brain, which generalizes to account, in part, for individual differences in stressor-evoked cardiovascular reactivity. In aggregate, these findings may have implications for understanding the neurophysiological mechanisms involved in linking psychological stress to CVD risk and stress-related clinical cardiovascular events.

Individual differences in stressor-evoked cardiovascular reactivity, particularly BP reactivity, have long been implicated in risk for CVD.[4,45] These individual differences are stable over time (ie, they show high repeatability) and are moderately generalizable from laboratory to daily life contexts, suggesting a trait-like phenotypic dimension of stress sensitivity and related CVD vulnerability.[41] There is now cumulative epidemiological evidence that stressor-evoked BP reactivity relates to increased prospective risk for a range of adverse cardiovascular outcomes independently of conventional cardiovascular risk factors, albeit with associations of modest effect size.[5] To better understand the mechanisms that may contribute to individual differences in stressor-evoked cardiovascular reactivity, this epidemiological work has been extended recently to neuroimaging studies that have attempted to characterize the intermediary brain systems and circuits that may link or transduce the processing (eg, appraisal) of psychological stressors to autonomic and neuroendocrine signaling along effector pathways that regulate the cardiovascular system. These studies have identified a number of brain areas that are capable of centrally orchestrating behavioral influences on CVD risk through peripheral physiological mechanisms.[13] Among the brain areas most consistently related in previous work to stressor-evoked cardiovascular reactivity—as well as some markers of autonomic cardiovascular control, inflammation, and arterial markers of preclinical vascular disease—are areas within the medial prefrontal cortex, anterior cingulate cortex, insula, extended amygdala, hippocampus, and hindbrain and brainstem cell groups.[1,13,16] It has been proposed that signaling patterns between these areas may serve to calibrate the magnitude of physiological (eg, cardiovascular) reactions to anticipated self-relevant demands (eg, stressors) to support contextually adaptive behavioral coping processes.[13,46,47] Moreover, an individual's propensity to exhibit "*mis*-calibrations" between brain and physiological activity may reflect a dimension of individual difference that underlies the expression of "exaggerated" (metabolically excessive or pathophysiological) autonomic, inflammatory, and cardiovascular reactions, including stressor-evoked BP reactions that have been linked to preclinical CVD.[46–48] In speculation, such "mis-calibrations" or "cardiovascular-metabolic uncoupling" may be reflected on the individual (person) level by a stronger expression of activity within the multivariate pattern identified in the present study.

In agreement with previous work, several so-called visceral control areas were encompassed by our multivariate brain pattern and were especially predictive of stressor-evoked cardiovascular reactivity, particularly areas within the medial prefrontal cortex, anterior cingulate cortex, and insula (see Figure 4; Tables S3 and S4). For example, Wager et al demonstrated that coordinated patterns of stressor-evoked activation in visceral control areas, including the medial prefrontal cortex and anterior cingulate cortex, accounted for concurrent HR reactions evoked by a threatening social evaluative stressor.[49,50] This study was extended recently in a reanalysis of data from 18 people, showing that cross-validated and multivariate brain patterns evoked by the social evaluative stressor reliably predicted concurrent HR and skin conductance changes.[51] Here, it is noteworthy that the particular multivariate brain pattern that predicted HR reactivity to social evaluative threat at the group level in that recent report accounted for ≈10% of the variance in HR reactivity across individuals (r=0.32±0.07). This effect size approximates that observed for the predictive association between the multivariate brain pattern derived in the present study and stressor-evoked BP reactivity (see Figure 3B). Moreover, several of the areas within the multivariate brain pattern that were predictive of HR reactivity to social threat encompassed core limbic areas for visceral control and stressor processing that were also observed to predict BP reactivity to cognitive stressors in the present study, including regions within the medial prefrontal cortex and anterior cingulate cortex. An important next step will be to determine the extent to which there is similarity or dissimilarity in multivariate brain patterns that predict different parameters of cardiovascular physiology that are evoked by cognitive stressors (used here) versus social evaluative tasks used in other stress testing paradigms.

In addition to canonical visceral control areas, our findings revealed other areas across the entire brain that were predictive of stressor-evoked cardiovascular reactivity (eg, within the cerebellum, motor cortex, and basal ganglia; see Figure 4; Tables S3 and S4), which is consistent with growing recognition that complex and brain-based processes are not reliably localizable to single areas, but to distributed circuits whose properties are arguably best quantified by multivariate or network-based methods.[52] In these regards, the present findings agree with, and extend extant results from, meta-analytic neuroimaging reviews of human autonomic and cardiovascular control.[12,18,19]

What are presently unclear, however, are the intermediate physiological mechanisms that might link stressor-evoked activity patterns in brain systems for autonomic and visceral control with acute changes in BP and other parameters of cardiovascular function. One such mechanism may involve acute changes in the operating characteristics of the baroreflex.[1,13,48,53] The baroreflex is a homeostatic control mechanism that constrains variability in BP on a beat-to-beat basis by adjusting parasympathetic and sympathetic outflow to the heart and vasculature by viscerosensory and visceromotor pathways that are subject to influence by areas within the forebrain, midbrain, and brainstem.[11] The autonomic adjustments that are induced by transient increases or decreases in BP lead to compensatory changes in HR, cardiac contractility, and vasoconstriction to alter subsequent levels of BP toward a homeostatic set point. Acute psychological stressors may alter or possibly "over-ride" the functioning of some components of the baroreflex, as evidenced most consistently by reductions in the gain or slope that defines the relationship between spontaneous and beat-to-beat changes in BP and "compensatory" changes in HR (ie, the cardiovagal baroreflex sensitivity).[13,48,54] A reduction in the sensitivity of this component of the baroreflex is thought to partly enable the simultaneous rise of BP with HR that is usually evoked by acute stressful experiences.[48,53] Psychological stressors may also affect other parameters of the baroreflex, including resetting effects on sympathetic vasomotor control over a higher operating range of BP,[1] but such effects have been less well studied in humans. Notably, it has been reported that individuals who exhibit greater stressor-evoked activation in forebrain, midbrain, and brainstem systems for autonomic and visceral control also exhibit a greater stressor-evoked reduction in cardiovagal baroreflex sensitivity.[55] Moreover, several of the areas previously reported to associate with stressor-evoked reductions in baroreflex sensitivity overlap with those that were predictive of stressor-evoked BP reactivity within the multivariate pattern (illustrated in Figure 4), including the dorsal and perigenual areas of the anterior cingulate cortex, ventromedial prefrontal cortex, and insula.

As supported by nonhuman animal evidence and findings from neuroimaging studies in humans, the anterior cingulate cortex, ventromedial prefrontal cortex, and insula, as well as other anatomically networked regions of the forebrain, midbrain, and brainstem, appear capable of altering viscerosensory and visceromotor control mechanisms of the baroreflex through their bidirectional communication with preautonomic cell groups.[1,13,16,54] Thus, it is possible that the predictive associations between activity changes in several brain areas encompassed within our multivariate pattern and stressor-evoked cardiovascular reactivity are mediated, in part, by centrally mediated influences on physiological control mechanisms, such as the baroreflex. However, an important next step will be determine whether relative activity *increases* or *decreases* in suspected brain systems for autonomic and visceral control relate to excitatory versus inhibitory neural processes that, in turn, affect intermediate physiological mechanisms that alter cardiovascular function. For instance, it has been suggested that activity increases in areas of the

ventromedial prefrontal cortex may be more consistently associated with increased parasympathetic cardiovascular control, whereas activity increases in areas of the perigenual and dorsal anterior cingulate may be more consistently associated with increased sympathetic cardiovascular control.[13,14,54] These suggestions appear compatible with the present observations that multivariate stressor-evoked activity weights in the ventromedial prefrontal cortex were negatively associated with BP reactivity, whereas those in the perigenual and dorsal portions of the anterior cingulate cortex were positively associated with BP reactivity (Figure 4). Such patterns of association could be attributable to the effects of decreased parasympathetic and increased sympathetic outflow to the heart and vasculature.

In addition to areas of the medial prefrontal cortex and anterior cingulate cortex, stressor-evoked activity changes in the insula were also predictive of BP reactivity (Figure 4; Tables S3 and S4). The latter observations accord with a corpus of nonhuman animal and human evidence for insular involvement in autonomic cardiovascular regulation through visceromotor and viscerosensory pathways (eg, involving baroreflex modulation), as well as the integration and coordination of peripheral physiology with cognitive and affective processes.[14,16,56] The functional neuroanatomy of the insula has been extensively reviewed, particularly with respect to its involvement in stress-related cardiovascular pathophysiology and clinical outcomes (eg, Takotsubo cardiomyopathy).[16,57] Based on existing evidence, it has been proposed that areas within the left insula may exhibit a stronger association with parasympathetic cardiovascular control, whereas areas in the right insula may exhibit a stronger association with sympathetic cardiovascular control.[16,19,58] Such autonomic control influences are enabled by dense insula connectivity with areas of the prefrontal cortex, anterior cingulate, hypothalamus, thalamus, medial temporal lobe (eg, amygdala, hippocampus), and cell groups within the midbrain and brainstem.[16] In these regards, specific observations from the present study appear consistent with proposed autonomic control functions ascribed to the left and right insula, wherein greater stressor-evoked BP reactivity was *negatively* associated with multivariate activity weights located in left insula and positively with those in right insula. The latter patterns of associations again could be explained by stressor-evoked and coordinated changes in networked forebrain areas that relate to decreases in parasympathetic and increases in sympathetic cardiovascular control. As noted above, more-precise measures of efferent (visceromotor) and afferent (viscerosensory) sympathetic and parasympathetic activity concurrent with fMRI and cardiovascular monitoring will help to determine these possibilities. Again, we emphasize, however, that both *positive* and *negative* predictive weights were distributed throughout the entire brain within the multivariate pattern, including putative areas for autonomic and visceral control (see Figure 3A). Thus, there is likely to be an intermixing of physiological (eg, sympathetic, parasympathetic) functions influenced by particular activity patterns within and across such networked areas.

Our findings are novel insofar as we have identified a multivariate pattern across the whole brain that may identify individuals exhibiting relatively greater stress sensitivity. Moreover, the methodological approach that was used to identify the whole-brain pattern may prove useful in other contexts to predict other dimensions of physiological stress responding and possibly clinical events. Hence, future studies may be able to identify individuals who more strongly exhibit a multivariate brain pattern that predicts clinically meaningful outcomes (eg, disease progression, new events, etc).[52] In a recent and foundational illustration of the plausibility of such a brain-based approach to predict CVD risk, Tawakol et al[59] demonstrated that elevated levels of basal metabolic activity within the amygdala predicted future CVD events above and beyond conventional CVD risk factors. An open question is whether multivariate and network-based approaches used in the present study would add to the predictive value of such single-region–based approaches and complement conventional CVD risk-prediction approaches. Moreover, it will be important to test whether adjunctive stress management interventions that are designed to protect against CVD risk[60] affect particular multivariate patterns of stress-related brain activity (brain biomarkers) linked to physiological mediators of CVD risk, including cardiovascular reactivity. If so, this would suggest the possible utility of surrogate brain biomarkers for use (eg, monitoring, intervention refinement, etc) in novel and neurobiologically informed intervention or prevention efforts in cardiovascular behavioral medicine.

We note that we used a standardized psychological stressor battery that was modeled after batteries used in epidemiological studies of stress-related CVD risk.[7] This stressor-battery controls for individual differences in task engagement and motor responding through performance titration procedures. We have also found, in previous work, that cardiovascular and behavioral responding to tasks of this battery is reliable across neuroimaging and laboratory-based testing contexts.[31] Accordingly, it may be appropriate for developing stress reactivity norms across a variety of populations. However, although the task may entail core dimensions of stressful experiences, including time pressure, loss of control, negative feedback, uncertainty, and conflict, it may lack direct correspondence to daily life stressors of personal or social relevance. Accordingly, future work in this area should use a range of stressors to test whether the brain pattern identified here is sensitive to diverse stressors or predicts other (eg, neuroendocrine) parameters of stress physiology across stressor contexts. In addition, clinical

cardiovascular events (eg, arrhythmia, ischemia) are also common under conditions of acute psychological stress,[61,62] and future work should determine whether the brain pattern identified here could, in part, account for the expression of clinical events through autonomic pathways.

We appreciate that the current sample consisted of an otherwise healthy group of midlife individuals who were mostly white, not on medications that could affect the cardiovascular system, and without a history of clinical CVD or other chronic illnesses, possibly limiting generalizability. In this regard, an important direction will be to determine whether the brain pattern identified here also predicts aspects of stress reactivity in diverse clinical and demographic samples across a range of contexts. We further appreciate that stress-related psychiatric disorders are highly comorbid with CVD and confer risk for future CVD events.[63] Thus, it may be possible to test whether individuals with these disorders more strongly exhibit the stress-related brain pattern identified here or whether an entirely different brain phenotype among these individuals accounts for some of the comorbidity between such psychiatric and cardiovascular outcomes. Finally, we note that there was appreciable variance in stressor-evoked cardiovascular reactivity that was unaccounted for by the multivariate brain pattern, and there was a decline in the accuracy of the pattern to predict increasingly greater levels of stressor-evoked cardiovascular reactivity. These observations underscore the need for model refinement in future work. Moreover, it will be important for future studies to simultaneously account for other possible sources of individual differences in cardiovascular reactivity, including genetic influences and individual differences in peripheral receptor sensitivity to autonomic and neuroendocrine outflow to the heart and vasculature.[2]

The present findings provide new evidence for a multivariate brain pattern that predicts individual differences in stressor-evoked cardiovascular reactivity. This suggests the possibility of an identifiable brain phenotype or brain biomarker that reflects stress-related CVD risk. This possibility agrees with recent findings demonstrating that brain activity linked to psychological stress forecasts clinical CVD events.[59] Accordingly, the present findings are relevant not only for furthering the understanding the neural bases of individual differences in cardiovascular stress physiology, but also for understanding the neural pathways that mechanistically link stressful experiences and CVD in at risk and clinical populations.

Sources of Funding

This work was supported by the National Institutes of Health (NHLBI R01-089850) and the National Science Foundation (DMS-1557572).

Disclosures

None.

References

1. Dampney RA. Central mechanisms regulating coordinated cardiovascular and respiratory function during stress and arousal. *Am J Physiol*. 2015;309:R429–R443.
2. Lovallo WR, Gerin W. Psychophysiological reactivity: mechanisms and pathways to cardiovascular disease. *Psychosom Med*. 2003;65:36–45.
3. Obrist PA. *Cardiovascular Psychophysiology: A Perspective*. New York, NY: Plenum; 1981.
4. Krantz DS, Manuck SB. Acute psychophysiologic reactivity and risk of cardiovascular disease: a review and methodologic critique. *Psychol Bull*. 1984;96:435–464.
5. Chida Y, Steptoe A. Greater cardiovascular responses to laboratory mental stress are associated with poor subsequent cardiovascular risk status: a meta-analysis of prospective evidence. *Hypertension*. 2010;55:1026–1032.
6. Carroll D, Ginty AT, Der G, Hunt K, Benzeval M, Phillips AC. Increased blood pressure reactions to acute mental stress are associated with 16-year cardiovascular disease mortality. *Psychophysiology*. 2012;49:1444–1448.
7. Jennings JR, Kamarck TW, Everson-Rose SA, Kaplan GA, Manuck SB, Salonen JT. Exaggerated blood pressure responses during mental stress are prospectively related to enhanced carotid atherosclerosis in middle-aged Finnish men. *Circulation*. 2004;110:2198–2203.
8. Brindle RC, Ginty AT, Phillips AC, Carroll D. A tale of two mechanisms: a meta-analytic approach toward understanding the autonomic basis of cardiovascular reactivity to acute psychological stress. *Psychophysiology*. 2014;51:964–976.
9. Ulrich-Lai YM, Herman JP. Neural regulation of endocrine and autonomic stress responses. *Nat Rev Neurosci*. 2009;10:397–409.
10. Saper CB. The central autonomic nervous system: conscious visceral perception and autonomic pattern generation. *Annu Rev Neurosci*. 2002;25:433–469.
11. Dampney RA. Functional organization of central pathways regulating the cardiovascular system. *Physiol Rev*. 1994;74:323–364.
12. Thayer JF, Ahs F, Fredrikson M, Sollers JJ III, Wager TD. A meta-analysis of heart rate variability and neuroimaging studies: implications for heart rate variability as a marker of stress and health. *Neurosci Biobehav Rev*. 2012;36:747–756.
13. Gianaros PJ, Wager TD. Brain-body pathways linking psychological stress and physical health. *Curr Dir Psychol Sci*. 2015;24:313–321.
14. Shoemaker JK, Norton KN, Baker J, Luchyshyn T. Forebrain organization for autonomic cardiovascular control. *Auton Neurosci*. 2015;188:5–9.
15. Myers B. Corticolimbic regulation of cardiovascular responses to stress. *Physiol Behav*. 2016;172:49–59.
16. Oppenheimer SM, Cechetto DF. Insular cortex and the regulation of cardiac function. *Compr Physiol*. 2016;6:1081–1133.
17. Critchley HD. Neural mechanisms of autonomic, affective, and cognitive integration. *J Comp Neurol*. 2005;493:154–166.
18. Vargas ER, Sörös P, Shoemaker JK, Hachinski V. Human cerebral circuitry related to cardiac control: a neuroimaging meta-analysis. *Ann Neurol*. 2016;79:709–716.
19. Beissner F, Meissner K, Bar KJ, Napadow V. The autonomic brain: an activation likelihood estimation meta-analysis for central processing of autonomic function. *J Neurosci*. 2013;33:10503–10511.
20. Worsley KJ, Friston KJ. Analysis of fMRI time-series revisited—again. *Neuroimage*. 1995;2:173–181.
21. Reddan MC, Lindquist MA, Wager TD. Effect size estimation in neuroimaging. *JAMA Psychiatry*. 2017;74:207–208.
22. Woo CW, Wager TD. What reliability can and cannot tell us about pain report and pain neuroimaging. *Pain*. 2016;157:511–513.
23. Kim SG. Quantification of relative cerebral blood flow change by flow-sensitive alternating inversion recovery (FAIR) technique: application to functional mapping. *Magn Reson Med*. 1995;34:293–301.
24. Sheu LK, Jennings JR, Gianaros PJ. Test-retest reliability of an fMRI paradigm for studies of cardiovascular reactivity. *Psychophysiology*. 2012;49:873–884.
25. Bradley MM, Lang PJ. Measuring emotion: the Self-Assessment Manikin and the Semantic Differential. *J Behav Ther Exp Psychiatry*. 1994;25:49–59.

26. Beck A, Steer R, Brown G. *Manual for the Beck Depression Inventory-II*. San Antonio, TX: Psychological Corporation; 1996.
27. Spielberger C, Gorsuch R, Lushene R. *STAI Manual for the State-Trait Anxiety Inventory*. Palo Alto, CA: Consulting Psychologists; 1970.
28. Barefoot JC, Dodge KA, Peterson BL, Dahlstrom WG, Williams RB Jr. The Cook-Medley hostility scale: item content and ability to predict survival. *Psychosom Med*. 1989;51:46–57.
29. Cook WW, Medley DM. Proposed hostility and pharisaic-virtue scales for the MMPI. *J Appl Psychol*. 1954;38:414–418.
30. Oldfield R. The assessment and analysis of handedness: the Edinburgh inventory. *Neuropsychologia*. 1971;9:97–113.
31. Gianaros PJ, Jennings JR, Sheu LK, Derbyshire SW, Matthews KA. Heightened functional neural activation to psychological stress covaries with exaggerated blood pressure reactivity. *Hypertension*. 2007;49:134–140.
32. Gianaros PJ, Sheu LK, Matthews KA, Jennings JR, Manuck SB, Hariri AR. Individual differences in stressor-evoked blood pressure reactivity vary with activation, volume, and functional connectivity of the amygdala. *J Neurosci*. 2008;28:990–999.
33. Diedrichsen J, Shadmehr R. Detecting and adjusting for artifacts in fMRI time series data. *Neuroimage*. 2005;27:624–634.
34. Kamarck TW, Everson SA, Kaplan GA, Manuck SB, Jennings JR, Salonen R, Salonen JT. Exaggerated blood pressure responses during mental stress are associated with enhanced carotid atherosclerosis in middle aged Finnish men: findings from the Kuopio Ischemic Heart Disease Study. *Circulation*. 1997;96:3842–3848.
35. Hastie T, Tibshirani R, Friedman J, Franklin J. The elements of statistical learning: data mining, inference and prediction. *Math Intell*. 2005;27:83–85.
36. Wager TD, Atlas LY, Leotti LA, Rilling JK. Predicting individual differences in placebo analgesia: contributions of brain activity during anticipation and pain experience. *J Neurosci*. 2011;31:439–452.
37. Zhao P, Rocha G, Yu B. The composite absolute penalties family for grouped and hierarchical variable selection. *Ann Stat*. 2009;37:3468–3497.
38. Efron R, Hastie T, Johston I, Tibshirani R. Least angle regression. *Ann Stat*. 2004;32:407–499.
39. Wager TD, Atlas LY, Lindquist MA, Roy M, Woo CW, Kross E. An fMRI-based neurologic signature of physical pain. *N Engl J Med*. 2013;368:1388–1397.
40. Jennings JR, Heim AF, Kuan DC, Gianaros PJ, Muldoon MF, Manuck SB. Use of total cerebral blood flow as an imaging biomarker of known cardiovascular risks. *Stroke*. 2013;44:2480–2485.
41. Kamarck TW, Lovallo WR. Cardiovascular reactivity to psychological challenge: conceptual and measurement considerations. *Psychosom Med*. 2003;65:9–21.
42. Akdeniz C, Tost H, Streit F, Haddad L, Wüst S, Schäfer A, Schneider M, Rietschel M, Kirsch P, Meyer-Lindenberg A. Neuroimaging evidence for a role of neural social stress processing in ethnic minority associated environmental risk. *JAMA Psychiatry*. 2014;71:672–680.
43. Tibshirani R. Regression shrinkage and selection via the lasso. *J R Stat Soc Series B Stat Methodol*. 1996;58:267–288.
44. Muscatell KA, Eisenberger NI. A social neuroscience perspective on stress and health. *Soc Personal Psychol Compass*. 2012;6:890–904.
45. Charvat J, Dell P, Folkow B. Mental factors and cardiovascular diseases. *Cardiologia*. 1964;44:124–141.
46. Gianaros PJ, Derbyshire SW, May JC, Siegle GJ, Gamalo MA, Jennings JR. Anterior cingulate activity correlates with blood pressure during stress. *Psychophysiology*. 2005;42:627–635.
47. Gianaros PJ, Sheu LK. A review of neuroimaing studies of stressor-evoked blood pressure reactivity: emerging evidence for a brain-body pathway to coronary heart disease risk. *Neuroimage*. 2009;47:922–936.
48. Ginty AT, Kraynak TE, Fisher JP, Gianaros PG. Cardiovascular and autonomic reactivity to psychological stress: neurophysiological substrates and links to cardiovascular disease. *Auton Neurosci*. 2017 Mar 16. pii: S1566-0702(17) 30069-3. DOI: 10.1016/j.autneu.2017.03.003. [Epub ahead of print].
49. Wager TD, Van Ast V, Hughes B, Davidson M, Lindquist MA, Ochsner KN. Brain mediators of cardiovascular responses to social threat, part II: prefrontal-subcortical pathways and relationship with anxiety. *Neuroimage*. 2009;47:836–851.
50. Wager TD, Waugh CE, Lindquist MA, Noll DC, Fredrickson BL, Taylor SF. Brain mediators of cardiovascular responses to social threat, part I: reciprocal dorsal and ventral sub-regions of the medial prefrontal cortex and heart-rate reactivity. *Neuroimage*. 2009;47:821–835.
51. Eisenbarth H, Chang LJ, Wager TD. Multivariate brain prediction of heart rate and skin conductance responses to social threat. *J Neurosci*. 2016;36:11987–11998.
52. Woo CW, Chang LJ, Lindquist MA, Wager TD. Building better biomarkers: brain models in translational neuroimaging. *Nat Neurosci*. 2017;20:365–377.
53. Berntson GG, Sarter M, Cacioppo JT. Anxiety and cardiovascular reactivity: the basal forebrain cholinergic link. *Behav Brain Res*. 1998;94:225–248.
54. Critchley HD, Harrison NA. Visceral influences on brain and behavior. *Neuron*. 2013;77:624–638.
55. Gianaros PJ, Onyewuenyi IC, Sheu LK, Christie IC, Critchley HD. Brain systems for baroreflex suppression during stress in humans. *Hum Brain Mapp*. 2012;33:1700–1716.
56. Critchley HD, Garfinkel SN. Interactions between visceral afferent signaling and stimulus processing. *Front Neurosci*. 2015;9:286.
57. Taggart P, Critchley H, van Duijvendoden S, Lambiase PD. Significance of neuro-cardiac control mechanisms governed by higher regions of the brain. *Auton Neurosci*. 2016;199:54–65.
58. Cechetto DF, Shoemaker JK. Functional neuroanatomy of autonomic regulation. *Neuroimage*. 2009;47:795–803.
59. Tawakol A, Ishai A, Takx RA, Figueroa AL, Ali A, Kaiser Y, Truong QA, Solomon CJ, Calcagno C, Mani V, Tang CY, Mulder WJ, Murrough JW, Hoffmann U, Nahrendorf M, Shin LM, Fayad ZA, Pitman RK. Relation between resting amygdalar activity and cardiovascular events: a longitudinal and cohort study. *Lancet*. 2017;389:834–845.
60. Blumenthal JA, Sherwood A, Smith PJ, Watkins L, Mabe S, Kraus WE, Ingle K, Miller P, Hinderliter A. Enhancing cardiac rehabilitation with stress management training: a randomized, clinical efficacy trial. *Circulation*. 2016;133:1341–1350.
61. Dimsdale JE. Psychological stress and cardiovascular disease. *J Am Coll Cardiol*. 2008;51:1237–1246.
62. Strike PC, Steptoe A. Systematic review of mental stress-induced myocardial ischaemia. *Eur Heart J*. 2003;24:690–703.
63. Rozanski A. Behavioral cardiology: current advances and future directions. *J Am Coll Cardiol*. 2014;64:100–110.

SUPPLEMENTAL MATERIAL

Table S1. The training sample (N = 206) vs. the test (cross-validation) sample (N = 104).

	Training Sample N = 206 106 Women, 100 Men		Test Sample N = 104 47 Women, 57 Men	
Characteristic	*Mean or (%)*	*SD or 95% CI*	*Mean or (%)*	*SD or 95% CI*
Age (years)	40.1	6.4	40.6	6.1
Race (%)				
Caucasian	70.4		71.2	
African American,	23.8		22.1	
Multi-racial, other	5.8		6.7	
Body mass index (kg/m^2)	26.9	5.2	26.7	4.6
Total cholesterol (mg/dL)	186.0	32.5	179.7	32.0
Triglycerides (mg/dL)	93.0	56.9	97.5	60.7
HDL (mg/dL)	51.6	17.7	49.0	13.1
Glucose (mg/dL)	88.7	11.0	88.6	10.7
Number of school years completed	16.8	3.4	16.5	3.1
Seated Resting SBP (mmHg)	120.4	9.8	120.8	9.9
Seated Resting DBP (mmHg)	71.9	8.3	73.5	8.8
Smoking Status (%)				
Current	16.5		17.3	
Former	21.4		16.3	
Never	62.1		66.3	
Depressive symptoms (BDI-II)	3.4	3.6	3.8	3.5
Trait anxiety (STAI-T)	32.5	7.3	33.8	7.6
Trait hostility (CMHS-T)	13.9	7.6	14.5	7.6
Task accuracy (% correct)				
MSIT congruent condition	91.1	7.9	91.8	4.2
MSIT incongruent condition	56.9	7.0	56.1	9.4
Stroop congruent condition	84.5	10.3	84.6	8.1
Stroop incongruent condition	55.7	9.8	55.0	11.1
Task reaction time (milliseconds)				
MSIT congruent condition	544.2	119.6	539.5	111.3
MSIT incongruent condition	902.7	198.1	894.9	211.6

Stroop congruent condition	1293.6	302.3	1313.3	287.8
Stroop incongruent condition	1861.4	485.4	1886.4	442.6
Changes from baseline in valence				
MSIT	-1.0	(-1.3, -0.8)	-1.4	(-1.7, -1.0)
Stroop	-1.5	(-1.8, -1.2)	-1.7	(-2.0, -1.4)
Changes from baseline in arousal				
MSIT	2.6	(2.2, 2.9)	2.6	(2.2, 3.0)
Stroop	3.0	(2.6, 3.3)	3.3	(2.8, 3.7)
Changes from baseline in SBP (mmHg)				
MSIT	3.5	(2.8, 4.2)	3.4	(2.3, 4.5)
Stroop	4.9	(4.0, 5.8)	5.0	(3.7, 6.3)
Changes from baseline in DBP (mmHg)				
MSIT	1.3	(0.7, 1.9)	1.5	(0.7, 2.3)
Stroop	2.1	(1.3, 2.8)	2.4	(1.6, 3.3)
Changes from baseline in HR (BPM)				
MSIT	5.9	(5.2, 6.7)	6.6	(5.6, 7.6)
Stroop	7.9	(7.0, 8.7)	8.6	(7.3, 9.9)

Note. Data are presented as number (or percentage), mean ± SD, or mean and 95% confidence interval (CI). HDL, high-density lipoproteins; LDL, low-density lipoproteins; SBP, systolic blood pressure; DBP, diastolic blood pressure; BDI-II, Beck Depression Inventory-II; STAI-T, State-Trait Anxiety Inventory-Trait version; CMHS-T, Cook-Medley Hostility Inventory-Trait version; MSIT, Multi-Source Interference Task.

Table S2. Stressor-evoked brain activation revealed at a family-wise error rate corrected threshold of P<0.05.

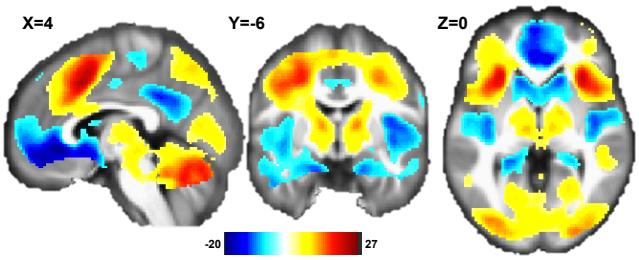

Effect	Region Label	Peak MNI Coordinates x	y	z	Peak t-value	Cluster Size
Positive	L/R Superior Medial Gyrus/Mid-ACC/dorsal ACC	±8	14	46	27.40	18707
	L/R Inferior Frontal Gyrus (pars Opercularis)	±40	4	28	24.08	
	L/R Anterior Insula	±32	22	4	22.90	
	L/R Precentral Gyrus	±30	0	52	22.02	
	L/R Middle Frontal Gyrus	±32	48	14	16.41	
	L/R Inferior Parietal Lobule	±30	-60	44	23.12	22787
	L/R Precuneus	±12	-72	48	21.43	
	L/R Middle Occipital Gyrus	±32	-80	20	20.04	
	L/R Superior Occipital Gyrus	-18	-70	44	19.40	
	L/R Cerebelum	±32	-68	-24	19.89	
	L/R Thalamus	±10	-16	6	16.30	752/845
	R Periaqueductal Gray	2	-28	-8	10.46	845
	R Middle Temporal Gyrus	48	-28	-8	11.62	128
Negative	L/R Rectal Gyrus/subgenual ACC	±12	10	-10	-20.75	5640
	L Rectal Gyrus/vmPFC/perigenual ACC	0	46	-16	-20.27	
	L/R Superior Frontal Gyrus	±16	40	48	-15.37	
	L/R Superior Medial Gyrus	±8	62	6	-12.79	
	L/R Middle Orbital Gyrus	±22	32	-16	-12.51	
	L/R Poster Cingulate Cortex	0	-42	34	-13.50	1056
	L/R Precuneus	±6	-56	20	-11.72	
	L/R Angular Gyrus	±52	-70	32	-20.06	695
	L/R Posterior Insula	±38	-18	16	-16.23	570
	L/R Mid- Occipital Gyrus	±54	-70	30	-16.13	286
	L/R Parahippocampal Gyrus/Hippocampus/Amygdala	±24	-16	-22	-15.81	869
	R Postcentral Gyrus	±48	-22	58	-11.64	130
	L Inferior Temporal Gyrus	±46	0	-36	-11.34	90
	R Superior Frontal Gyrus	20	42	48	-11.06	214
	L Middle Temporal Gyrus	-56	-12	-20	-10.37	84

Note. Regions were labeled using bspmview (https://github.com/spunt/bspmview). ACC, anterior cingulate cortex; vmPFC, ventromedial prefrontal cortex.

Table S3. Regions within the whole-brain multivariate weight map that positively predicted stressor-evoked SBP reactivity after applying a permutation threshold of P<0.05 and a voxel extent threshold of k=50 (1000 permutations). Note that the whole-brain pattern was used in training and testing as described in the text.

Region Label	Extent	t-value	x	y	z
L Middle Temporal Gyrus	255	4.163	-68	-24	-12
L Paracentral Lobule	783	3.877	-18	-24	70
R Postcentral Gyrus	694	3.565	44	-24	54
L Superior Occipital Gyrus	1042	3.406	-18	-72	34
R Inferior Temporal Gyrus	454	3.399	60	-50	-18
R Dorsal Anterior Cingulate	301	3.387	8	36	26
R Insula	421	2.793	34	24	14
R Rolandic Operculum	72	3.343	68	0	20
R Cerebellum/Periaqueductal Gray	96	3.342	18	-28	-20
R Cerebellar Vermis	126	3.312	6	-62	-26
L Dorsal Anterior Cingulate	68	3.236	-2	22	16
L Inferior Occipital Gyrus	113	3.146	-52	-78	0
R Linual Gyrus	51	3.140	8	-58	8
R Cerebelum	58	3.122	32	-86	-22
L Rolandic Operculum	141	3.110	-40	-14	22
R Fusiform Gyrus	111	3.107	38	-10	-30
L Middle Frontal Gyrus	164	3.055	-34	10	56
R Middle Frontal Gyrus	167	3.052	34	14	44
L Middle Frontal Gyrus	146	3.035	-24	30	32
R Mid Orbital Gyrus, perigenual ACC	192	3.028	10	50	-4
L Cerebelum	86	2.955	-18	-88	-32
L Inferior Parietal Lobule	71	2.940	-36	-50	38
R Cerebellum	62	2.937	26	-34	-46
L Superior Orbital Gyrus	202	2.934	-12	62	0
L Superior Frontal Gyrus	202	2.164	-30	66	10
R Inferior Temporal Gyrus	102	2.926	42	-58	-4
R Cerebelum	51	2.924	18	-62	-16
R Posterior Mid-Cingulate	82	2.917	4	-44	48
R Precentral Gyrus	70	2.904	36	-14	44
L Lingual Gyrus	127	2.895	-2	-94	-14
L Inferior Temporal Gyrus	186	2.835	-38	-42	-10
L IFG (p. Triangularis)	50	2.731	-56	30	6
R ParaHippocampal Gyrus	119	2.723	30	-42	-2
R Paracentral Lobule	63	2.714	10	-36	58
L IFG (p. Triangularis)	138	2.685	-54	28	22
L Cerebelum	98	2.646	-46	-50	-30
R Precuneus	97	2.620	10	-68	50
R Posterior Mid-Cingulate	54	2.612	2	-16	40
L Mid Orbital Gyrus, Anterior Cingulate	64	2.577	-2	42	0
R Superior Medial Gyrus	54	2.534	4	52	8
R Parahippocampal Gyrus	52	2.509	36	-34	-8
R Middle Temporal Gyrus	121	2.473	50	-70	26
R Superior Medial Gyrus	65	2.456	6	54	46
R IFG (p. Orbitalis)	50	2.347	36	30	-16
R Supramarginal Gyrus	103	2.336	68	-26	30
L Superior Temporal Gyrus	54	2.319	-64	-36	26

Table S4. Regions within the whole-brain multivariate weight map that negatively predicted stressor-evoked SBP reactivity after applying a permutation threshold of P<0.05 and a voxel extent threshold of k=50. Note that the whole-brain pattern was used in training and testing as described in the text.

Region Label	Extent	t-value	x	y	z
L Paracentral Lobule	256	-4.030	-4	-42	78
L Posterior Cingulate Cortex	295	-3.761	-2	-50	12
R Superior Frontal Gyrus	237	-3.633	30	-10	64
L Middle Temporal Gyrus	267	-3.618	-58	-54	12
R Middle Frontal Gyrus	62	-3.590	40	52	30
R Hippocampus	100	-3.418	32	-20	-12
L Cerebelum	143	-3.380	-18	-64	-36
R Lingual Gyrus	138	-3.325	10	-78	2
Medial Occipital Lobe	127	-3.316	0	-96	-20
R Inferior Temporal Gyrus	62	-3.309	52	-20	-36
L Superior Frontal Gyrus	137	-3.295	-26	54	36
L Fusiform Gyrus	110	-3.268	-26	-20	-46
R Superior Medial Gyrus	60	-3.256	8	70	16
L Inferior Temporal Gyrus	53	-3.247	-52	-30	-30
R Middle Temporal Gyrus	161	-3.216	64	-36	0
L Calcarine Gyrus	284	-3.214	-6	-98	2
L Thalamus	50	-3.200	-14	-28	10
R IFG (p. Opercularis)	169	-3.084	52	12	40
L Anterior Insula, L IFG (p. Orbitalis)	290	-3.076	-46	18	-6
L Putamen	92	-3.064	-18	20	-4
L Medial Temporal Pole	130	-3.063	-36	14	-32
L Fusiform Gyrus	96	-3.015	26	-18	-34
L Superior Medial Gyrus	107	-3.009	2	26	54
R Superior Temporal Gyrus	122	-2.952	56	-36	18
R Brainstem, Pons	194	-2.952	12	-40	-34
L Temporal Pole	59	-2.937	-34	4	-50
L Fusiform Gyrus	160	-2.935	-22	-36	-16
R Cerebelum	73	-2.926	14	-90	-40
L Superior Temporal Gyrus	92	-2.865	-38	-38	16
L Inferior Parietal Lobule	261	-2.859	-52	-54	48
L Angular Gyrus	261	-2.583	-32	-56	42
L Superior Temporal Gyrus	261	-2.537	-64	-54	28
R Middle Temporal Gyrus	53	-2.859	42	-60	12
L Cerebellum	108	-2.849	-50	-72	-42
L Gyrus, Rectus, Ventromedial Prefrontal Cortex	123	-2.845	-6	48	-24
L Superior Orbital Gyrus	123	-2.306	-8	24	-20
L Middle Frontal Gyrus	64	-2.825	-44	18	44
L Supplementary Motor Area	100	-2.811	-2	6	50
R Middle Occipital Gyrus	85	-2.728	38	-90	12
R Cerebelum	226	-2.725	52	-64	-40
R Putamen	164	-2.720	18	8	-4
R Middle Temporal Gyrus	138	-2.713	60	-58	22
L Fusiform Gyrus	73	-2.699	-24	-50	-10
R Cerebelum	50	-2.673	30	-52	-16
R Supramarginal Gyrus	113	-2.666	54	-38	44
L Precentral Gyrus	54	-2.632	-50	2	22
L Paracentral Lobule	81	-2.599	-10	-22	54

L Inferior Temporal Gyrus	53	-2.478	-52	-12	-22
R Lingual Gyrus	74	-2.418	24	-98	-14
L Angular Gyrus	56	-2.369	-42	-76	44

Note: t-values were determined by 1000 random permutations of Y vs. X to compute the standard deviation of the whole brain multivariate pattern under the null hypothesis of no association between the pattern and SBP reactivity. Regions were labeled in bspmview (https://github.com/spunt/bspmview). ACC, Anterior Cingulate Cortex; IFG: inferior frontal gyrus.

Figure S1. Machine learning methods and cross-validation.

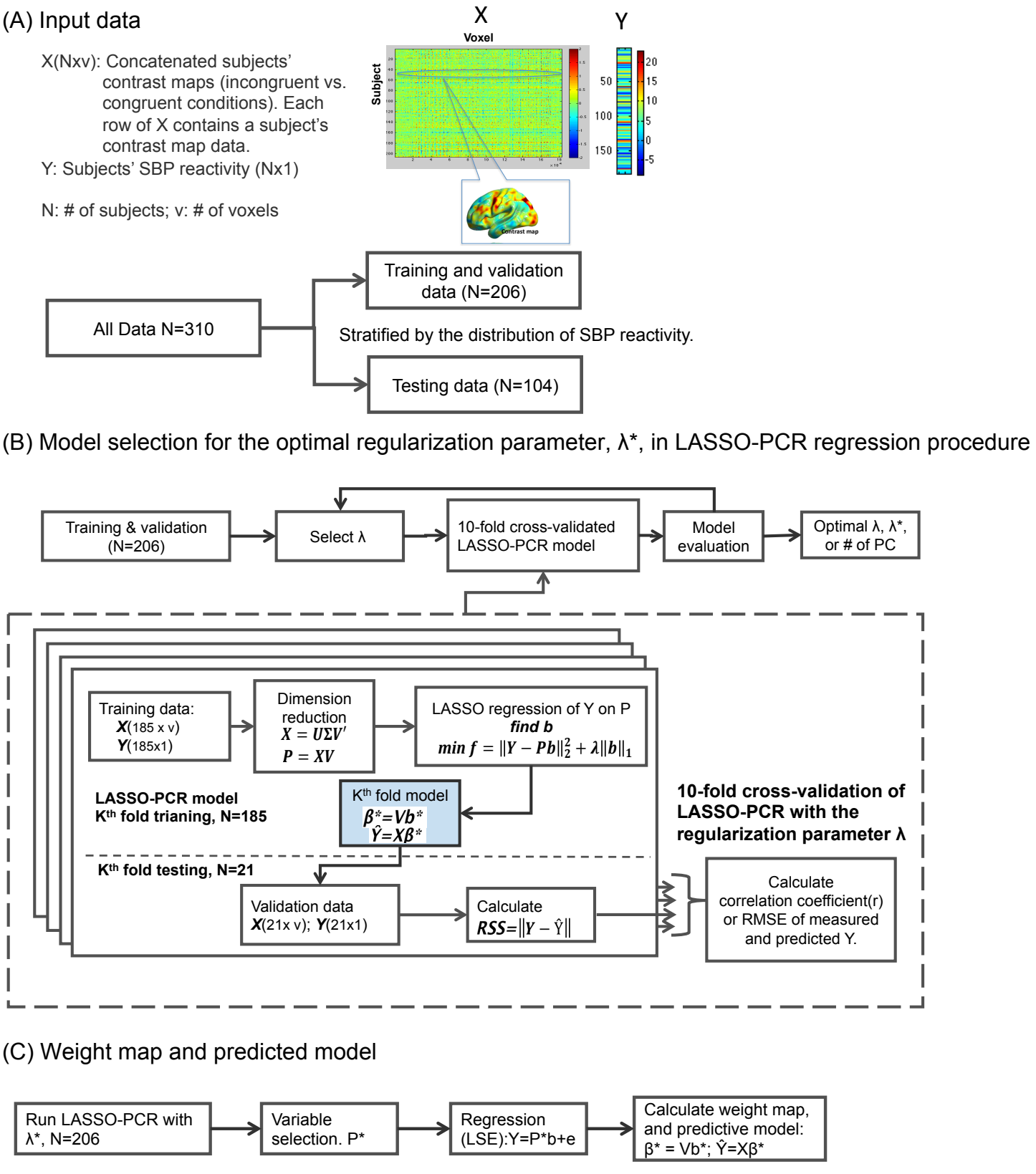

(D) Model performance testing

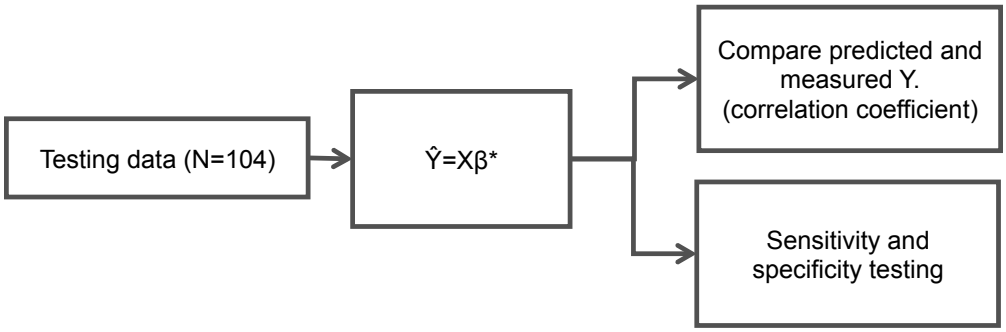

Figure S1. Schematic of machine learning procedure using LASSO-PCR, with 10-fold cross-validation. (A) Input data. (B) In each fold, k, k=1,..10, brain activation maps from the training sample were concatenated (X) and converted to a principal components' matrix, P, for a penalized regression model predicting SBP reactivity (Y) on P. LASSO with a regularization parameter, λ, between 0 and 1 was used to fit the model. The fitted model was used to predict Y in the validation sample and compute the residual sum of square (RSE) for each fold. The root mean square error (RMSE), as well as the correlation of the predicted and measured Y, was summarized from all folds. The best λ that yielded the smallest RMSE was selected. (C) The regression of Y on the principal components was run with the best λ. Ordinary least square estimation was applied to fit the regression of Y on the selected components. The estimated coefficients were projected back to 3D voxel space to derive the final multivariate pattern (weight map, β*) to predict SBP reactivity (y), $y = x \beta^*$. (D) As described in the Methods of the main text, the model was tested for accuracy using a separate and independent sample of subjects not used for training, the test sample.

A Brain Phenotype for Stressor–Evoked Blood Pressure Reactivity

Peter J. Gianaros, Lei K. Sheu, Fatma Uyar, Jayanth Koushik, J. Richard Jennings, Tor D. Wager, Aarti Singh and Timothy D. Verstynen

J Am Heart Assoc. 2017;6:e006053; originally published August 23, 2017;
doi: 10.1161/JAHA.117.006053
The *Journal of the American Heart Association* is published by the American Heart Association, 7272 Greenville Avenue, Dallas, TX 75231
Online ISSN: 2047-9980